

# PoseNet3D: Unsupervised 3D Human Shape and Pose Estimation

Shashank Tripathi\* Siddhant Ranade\* Amrish Tyagi Amit Agrawal  
Amazon Lab126

{shatripa, srranade, ambrisht, aaagrawa}@amazon.com

## Abstract

*Recovering 3D human pose from 2D joints is a highly unconstrained problem. We propose a novel neural network framework, PoseNet3D, that takes 2D joints as input and outputs 3D skeletons and SMPL body model parameters. By casting our learning approach in a student-teacher framework, we avoid using any 3D data such as paired/unpaired 3D data, motion capture sequences, depth images or multi-view images during training. We first train a teacher network that outputs 3D skeletons, using only 2D poses for training. The teacher network distills its knowledge to a student network that predicts 3D pose in SMPL representation. Finally, both the teacher and the student networks are jointly fine-tuned in an end-to-end manner using temporal, self-consistency and adversarial losses, improving the accuracy of each individual network. Results on Human3.6M dataset for 3D human pose estimation demonstrate that our approach reduces the 3D joint prediction error by 18% compared to previous unsupervised methods. Qualitative results on in-the-wild datasets show that the recovered 3D poses and meshes are natural, realistic, and flow smoothly over consecutive frames.*

## 1. Introduction

Accurately estimating 3D pose from 2D landmarks is a classical ill-posed problem in computer vision [15, 21]. Previous methods for 3D pose prediction can be classified into model-free and model-based approaches. Typically, model-free approaches directly learn a mapping from 2D landmarks to 3D joints [6, 9, 39, 40]. Predicting 3D joints from 2D landmarks (lifting) is a challenging task, since there exists an infinite number of 3D poses corresponding to a 2D skeleton due to projective ambiguity [6]. Model-based approaches often fit 3D parametric models such as SMPL [37] to estimate 3D shape and pose. This is typically done by minimizing the 2D error between the projection of the predicted 3D pose and the given 2D landmarks. However, as

shown in [27], 2D reprojection error alone is highly under-constrained and can be minimized via non-natural joint angles. To address these issues, previous 2D to 3D approaches have used various kinds of additional 3D supervision, including paired 2D-3D correspondences [39], unpaired 3D data [27] and synthetic data generated using motion capture (MoCap) sequences [51].

In this paper, our goal is to train a neural network that takes 2D pose (landmarks) as input and outputs SMPL parameters and 3D skeletons, without requiring any additional 3D data or iterative fitting during training. We first train a lifting network (aka teacher) using only 2D inputs to predict *model-free* 3D poses. The 3D pose output from the teacher is then used as pseudo ground-truth to train a student network to predict SMPL pose parameters. Thus, inspired by the knowledge distillation (KD) framework, our teacher-student formulation allows training the network in the absence of additional 3D data. In fact, we show that training the student network by directly minimizing the 2D reprojection error (without using knowledge from the teacher) fails due to inherent ambiguities in 2D projection, resulting in incorrect depth predictions and unnatural poses.

Optimization based approaches such as [2] can also fit SMPL meshes to 2D poses. However such approaches are computationally expensive, potentially prone to error and require good initialization as well as 3D pose priors built using MoCap sequences. In contrast, our teacher-student formulation allows training a feed-forward network that can directly output SMPL pose for a given 2D input.

Typically, KD approaches train the teacher network in a supervised manner and the student network is often used to reduce run-time/complexity. Our approach builds upon [6] and trains the teacher (lifter) network in an unsupervised manner without using multi-view images [53, 56], depth images [54], or 3D supervision. Compared to previous works, we show improvement by utilizing dilated convolutions to model temporal dynamics.

When using a parametric model such as SMPL, there often exists a semantic gap between the SMPL 3D joints and the 2D landmarks obtained from RGB images (e.g. using OpenPose [4]). For example, the 3D hip joints in

\*Equal Contribution

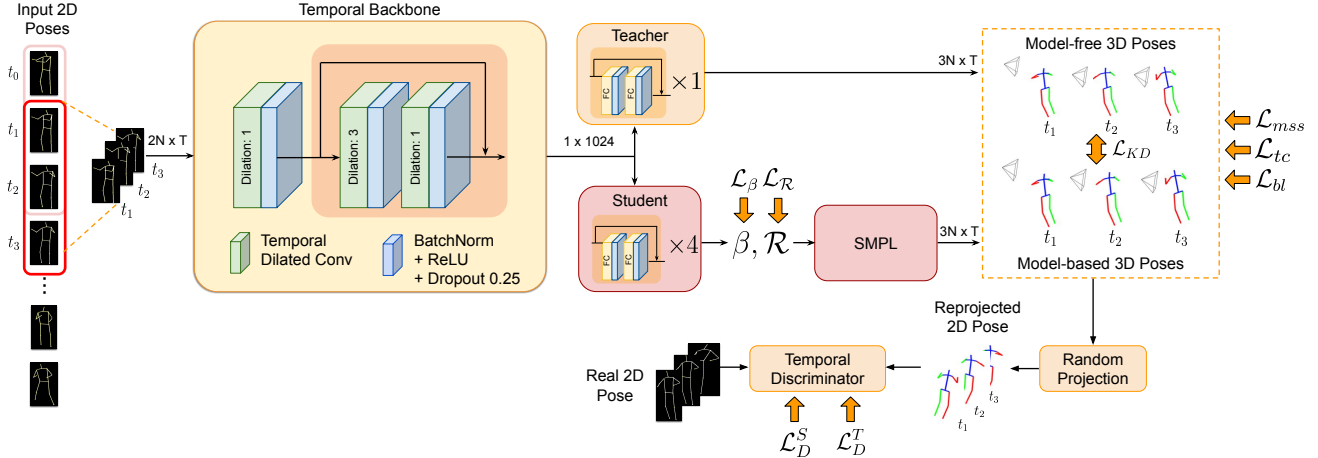


Figure 1: Overview of the proposed PoseNet3D approach. Input 2D poses are fed to a temporal backbone, followed by a teacher branch and a student branch, which outputs model-free 3D poses and SMPL parameters respectively.

SMPL are close to the center of the pelvis, while in the Human3.6M [23] dataset, the 2D hip joints are close to the body surface. In previous works, this semantic adaptation is learned offline by fitting SMPL meshes to specific 3D datasets and is used during evaluation. Thus, 3D data is also required implicitly for bridging the aforementioned semantic gap. In contrast, we demonstrate that the semantic adaptation can be automatically learned during training to bridge the gap between the SMPL 3D joints and the 2D landmarks during training. Bridging this semantic gap, which is often ignored in previous works is crucial, otherwise the network can minimize joint error by twisting the body, resulting in unnatural poses.

We evaluate our approach on 3D human pose estimation tasks on Human3.6M and MPI-INF-3DHP datasets, reducing the mean per joint position error by 18% compared to the state-of-the-art unsupervised method of [6] (47mm vs 58mm) as shown in Sect. 4. Qualitative results confirm that our method is able to recover complex 3D pose articulations on previously unseen in-the-wild images (e.g. Fig. 4).

## 2. Related Work

Several deep learning techniques have been proposed to estimate 3D joints directly from 2D images [7, 8, 18, 24, 36, 42, 47, 48, 50, 57, 58, 64, 70, 71]. We build upon approaches that decompose the problem into estimation of 2D joints from images followed by the estimation of 3D pose. Obtaining 2D joints from images is a mature area in itself and several approaches such as CPM [65], Stacked-Hourglass (SH) [44], Mask-RCNN [19] or affinity models [4] can be used.

Previous 2D to 3D approaches can be broadly classified into (a) model-free methods and (b) model-based methods. Model-free methods [3, 5, 6, 13, 14, 25, 39, 43] predict a 3D skeleton from 2D joints. Model-based approaches use a

parametric model such as SMPL to estimate human meshes. Several model-free as well as model-based approaches have used 3D supervision during training. The 3D information has been used in various forms such as paired 2D-3D data [5, 25, 34, 39, 41, 43, 52], 3D pose priors (e.g. Gaussian Mixture Model) built using 3D MoCap sequences [2, 31], learned priors using 3D data via discriminator [27], and synthetic 2D-3D pairings [51, 67]. Our key contribution is a novel combination of model-based and model-free predictions, without requiring additional 3D data during training.

Approaches such as [6, 56, 63] have primarily used 2D joints from single/multi-view images without explicit 3D supervision to learn 3D pose. Chen *et al.* [6] proposed an unsupervised algorithm for lifting 2D poses to 3D. Their key intuition is that random 2D projections of accurately estimated 3D pose should conform to the real 2D pose distribution. A 2D discriminator is used to give feedback to the lifter about the naturalness of random 2D projections of the predicted 3D skeleton. This helps training the lifter without requiring direct 3D supervision.

Our teacher network builds upon the work of Chen *et al.* [6], but differs in the following respects. Firstly, in [6], inference uses a single frame as input and weak temporal consistency is enforced using an additional discriminator on frame differences. Their architecture only employs fully connected layers. In contrast, we use dilated convolutions (similar to [52]) to model temporal dynamics in the lifter as well as in the discriminator and train/test on multi-frame inputs. Video based approaches such as Li *et al.* [35] employ 3D trajectory optimization via low rank property and temporal smoothness of video sequences. Instead, we propose novel loss terms to account for the consistency of predicted skeletons on common frames across neighboring time-steps and show improvement in accuracy on the Human3.6M dataset over [6]. Secondly, unlike [6], our ap-

proach is also able to estimate SMPL parameters.

**Deep Learning with SMPL:** Deep learning approaches such as [1, 27, 31, 38, 45, 49, 51, 59, 61] have utilized SMPL to directly regress to the underlying shape and pose parameters by training a feed-forward network. The 3D joints are computed via linear regression on the estimated mesh vertices [27]. Our student network also predicts SMPL parameters but differs from these approaches in following respects.

Firstly, approaches such as [27] minimize the 2D re-projection error between the projection of the SMPL 3D joints and the predicted 2D joints from images. However, as noted in [27], 2D keypoint loss is highly unconstrained and thus [27] learns the limits of joint angles using a dataset of 3D scans. This is done by training a discriminator to bring the distribution of predicted SMPL parameters close to the real distribution of SMPL parameters obtained from 3D scans. Since we do not assume access to any additional 3D data at training time, we address this problem by first training a teacher network to predict 3D joint positions. We then use the output of the teacher as pseudo ground-truth to train the student network to predict SMPL parameters. By using knowledge distillation from the teacher along with simple regularizers on the SMPL parameters, we can recover realistic 3D pose without requiring additional 3D information during training. Our ablation studies show that the proposed strategy significantly outperforms the baseline strategy of directly minimizing the 2D re-projection error.

Secondly, previous works typically ignore the semantic gap between the SMPL 3D joints and the 2D landmarks while training. Instead, a regressor from vertices to joints [1, 12, 27] is obtained offline by fitting SMPL meshes to specific 3D datasets (e.g. Human3.6M). In contrast, we bridge this gap using *semantic joint adaptation* (SJA) during training of the student network. We demonstrate that SJA improves the accuracy as well as naturalness of the predicted 3D pose.

**SMPL based Optimization:** Classical optimization techniques has also been used previously to fit the SMPL model to image evidence given by 2D landmarks/silhouettes [2, 17, 33, 41]. The optimization based approaches are typically slow and prone to error. In contrast, our approach trains a feed-forward network allowing for a faster and more robust inference. Recently, Kolotouros *et al.* [31] (*SPIN*) have used iterative optimization within the training loop of a deep neural network to generate pseudo ground-truth, which is used to provide direct supervision on SMPL parameters for regression. Instead, our teacher network provides supervision on 3D joints, obtained by SMPL forward kinematics. In contrast to *SPIN*, we do not use a 3D pose prior learned using CMU MoCap sequences (similar to [2]). Our approach can also be extended to use optimization in the loop to generate additional supervision on SMPL pa-

rameters, which we leave for future work.

**Knowledge Distillation:** Distilling the knowledge in neural networks has been used for applications such as network compression, combining an ensemble of models into a single model [20], enhancing privacy [46], large scale semi-supervised learning [68] *etc.* Wang *et al.* [63] use non-rigid structure from motion (NRSfM) algorithm as the teacher to learn 3D pose from 2D joints. In contrast, we use a 2D-3D lifter as a teacher and show better results on Human3.6M. Unlike [63], our approach also outputs SMPL parameters.

### 3. Proposed Approach

Our PoseNet3D approach is a combination of model-free 3D pose estimation followed by knowledge distillation to predict SMPL pose parameters. As shown in Fig. 1, the input to our network is a set of  $T$  2D skeletons from  $T$  consecutive frames of a video. The architecture consists of a temporal backbone, which utilizes dilated convolutions over time to model the temporal dynamics and produces a feature vector. The feature vector is fed to two branches: (a) Teacher branch, which outputs 3D poses, and (b) Student branch, which outputs SMPL parameters. The 3D joints from the student branch are computed as described in Section 3.3. The two sets of 3D joints from the student and teacher branches are compared to ensure consistency. The predicted 3D joints from the teacher and the student branches are re-projected to 2D after random rotations and are fed to a temporal discriminator. In the following sections, we describe the teacher and student networks and associated training losses in detail.

#### 3.1. Teacher: Temporally Consistent Lifting

Let  $\mathbf{x}_i^j = (x_i^j, y_i^j), i = 1, \dots, N$  denote the  $i^{th}$  2D pose landmark of a skeleton in frame  $j$  with the root joint (mid-point between the hip joints) as origin. The 2D skeleton for frame  $j$  is  $\mathbf{x}^j = \{\mathbf{x}_1^j, \dots, \mathbf{x}_N^j\}$ . The input to the network at time step  $t$  is a set of  $T$  2D skeletons represented as  $\mathbf{x}(t) = \{\mathbf{x}^t, \dots, \mathbf{x}^{T-t+1}\}$ . For simplicity, we drop the dependence on time-step to describe the lifter. Similar to [6], we assume a perspective camera with unit focal length centered at the origin and fix the distance of the 3D skeleton to the camera to a constant  $c$  units. The 2D skeletons are normalized such that the mean distance from the head joint to the root joint is  $\frac{1}{c}$  units in 2D.

At each time-step  $t$ , the temporal lifting branch predicts a depth offset  $o_i^j$  for each  $\mathbf{x}_i^j$ . The 3D joints are computed as  $\mathbf{X}_i^j = (x_i^j z_i^j, y_i^j z_i^j, z_i^j)$ , where  $z_i^j = \max(1, c + o_i^j)$ . The generated skeletons are projected back to 2D via random projections. Let  $\mathbf{Q}$  be a random rotation matrix. The rotated 3D skeleton  $\mathbf{Y}_i^j$  is obtained as

$$\mathbf{Y}_i^j = \mathbf{Q}(\mathbf{X}_i^j - \mathbf{X}_r^j) + \mathbf{C}, \quad (1)$$

where  $\mathbf{X}_i^j$  is the predicted root joint of  $j^{\text{th}}$  skeleton and  $\mathbf{C} = (0, 0, c)^T$ . Let  $\mathbf{y}_i^j$  denote the 2D projection of  $\mathbf{Y}_i^j$ .

### 3.2. Training Losses for the Teacher Network

**Multi-Frame Self-Supervision Loss:** Let  $\mathcal{G}_T$  denote the teacher network that predicts the model-free 3D pose  $\mathbf{X}_i^j = \mathcal{G}_T(\mathbf{x}_i^j)$  as defined in Section 3.1. We also lift the reprojected 2D skeletons to obtain  $\tilde{\mathbf{Y}}_i^j = \mathcal{G}_T(\mathbf{y}_i^j)$  using the same network. If  $\mathcal{G}_T(\cdot)$  is accurate,  $\tilde{\mathbf{Y}}_i^j$  should match  $\mathbf{Y}_i^j$ . Therefore, we define our multi-frame self-supervision loss as

$$\mathcal{L}_{mss} = \sum_i^N \sum_j^T \|\mathbf{Y}_i^j - \tilde{\mathbf{Y}}_i^j\|^2. \quad (2)$$

**Temporal Consistency Loss:** Since we predict  $T$  3D skeletons at each time step  $t$ , common frames exist between neighboring time-steps. Using a sliding window with temporal stride 1, we have  $T - 1$  frames in common between time-step  $t$  and  $t + 1$ . We use an  $\mathcal{L}_2$  loss to enforce consistency between these common frames in 3D,

$$\mathcal{L}_{tc} = \sum_{j=1}^{T-1} \|\mathbf{X}_i^{j+1}(t) - \mathbf{X}_i^j(t+1)\|^2. \quad (3)$$

**Bone Length Loss:** At each time step  $t$ , we enforce that the bone lengths for the  $T$  predicted 3D skeletons be consistent by minimizing the variance of bone lengths over the  $T$  frames. Let  $b(m, n, j) = \|\mathbf{X}_m^j - \mathbf{X}_n^j\|$  denote the bone length between the  $m^{\text{th}}$  and  $n^{\text{th}}$  predicted 3D joints for frame  $j$ . Bone length loss is defined as

$$\mathcal{L}_{bl} = \sum_{m=1}^N \sum_{n \in \mathcal{N}(m)} \text{Var}_j(b(m, n, j)), \quad (4)$$

where  $\mathcal{N}(m)$  denotes the set of connected skeleton joints for joint  $m$  and  $\text{Var}_j$  denotes variance over  $T$  frames.

**Temporal Discriminator:** The discriminator provides feedback to the lifter regarding the realism of projected 2D skeletons. In contrast to [6], which uses a single frame discriminator and a frame-difference discriminator, we use a *single* temporal discriminator that takes a set of  $T$  reprojected/real 2D skeletons as input. Previous approaches have used RNN and LSTM to model sequential/temporal data. A challenge in using RNN/LSTM is delayed feedback which requires the use of a policy gradient to back-propagate the feedback from the discriminator [11]. In contrast, our temporal discriminator uses dilated convolutions and provides feedback at each time-step, simplifying the training. Formally, the discriminator is trained to distinguish between sequences of  $T$  real 2D skeletons  $\mathbf{r}(t) = \{\mathbf{r}^1, \dots, \mathbf{r}^T\}$  (target probability of 1) and fake (projected) 2D skeletons

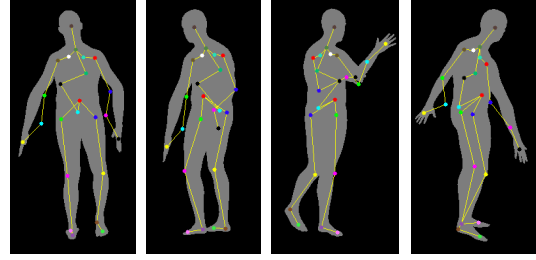


Figure 2: Linear correction on SMPL 3D joints for SJA (Equation 6) could lead to network placing joints outside the mesh. Visualization shows rendering of predicted mesh with projection of 3D joints overlaid on top.

$\mathbf{y}(t) = \{\mathbf{y}^1, \dots, \mathbf{y}^T\}$  (target probability of 0). We utilize a standard adversarial loss [16] defined as

$$\mathcal{L}_D^T = \min_{\Theta_T} \max_{\Theta_D} \mathbb{E}(\log(D(\mathbf{r}(t))) + \log(1 - D(\mathbf{y}(t)))), \quad (5)$$

where  $\Theta_T$  and  $\Theta_D$  denote the parameters of the teacher and the discriminator networks, respectively.

### 3.3. Student: Estimating SMPL Parameters

For our model-based approach, we use the Skinned Multi-Person Linear (SMPL) representation [37]. SMPL is a parametric model that factors human bodies into a shape (body proportions) and pose (articulation) representation. The shape is parameterized using a PCA subspace with 300 basis shapes and shape coefficients ( $\beta$ ). The human pose is modeled as a set of 24 local joint angles corresponding to  $K = 24$  3D joints (including root joint) and is represented as 72 axis-angle coefficients. We directly predict the rotation matrix corresponding to each joint from the network, on which we perform a differentiable ortho-normalization. Let  $\mathcal{R} = \{R_1, \dots, R_K\}$  denote the set of  $K$  rotation matrices. Given a set of parameters  $\beta$  and  $\mathcal{R}$ , SMPL produces a mesh  $V = \mathcal{M}(\beta, \mathcal{R}), V \in \mathbb{R}^{6890 \times 3}$  with 6890 vertices, where  $\mathcal{M}$  is differentiable. Note that the 3D joints by themselves do not fully constrain the shape of the body and it is not possible to predict accurate shape using 3D joints alone. Approaches such as [51] have additionally used silhouettes to estimate shape and thus accurate shape prediction is not a goal of this paper. We only predict the first 10  $\beta$  parameters (common for all  $T$  frames) and set the remaining to zero. Thus, the student network has a total of  $10 + 24 \times 9 \times T = 10 + 216 \times T$  outputs at each time step.

#### 3.3.1 Semantic Joint Adaptation (SJA)

The 3D joints  $J \in \mathbb{R}^{24 \times 3}$  are obtained by linear regression from the final mesh vertices  $V$ . The linear regressor is a sparse matrix  $W \in \mathbb{R}^{24 \times 6890}$ , which represents a convex combination of vertices for each 3D joint. Hence,  $J = WV$ . The pre-trained linear regressor in SMPL produces 3D joints that are often semantically different from

the 2D joints obtained from 2D pose detectors or annotations on datasets. For example, in SMPL the 3D hip joints are closer to the center of the body. However, in Human3.6M 2D annotations, the hip landmarks are closer to the periphery. Our SJA module learns the adaptation of the SMPL 3D joints to 2D joints used for training.

We first experimented with a linear layer that learns a weight matrix  $A \in \mathbb{R}^{72 \times 72}$  and an bias vector  $\mathbf{b} \in \mathbb{R}^{72 \times 1}$ , which is applied to the  $72 \times 1$  vectorized representation of  $J$  to adapt the SMPL joints (referred to as *Linear-SJA*),

$$\mathbf{J}' = \mathbf{A}\mathbf{J} + \mathbf{b}. \quad (6)$$

However, such an approach fails in practice. Since there is no constraint on joints, the network can potentially learn to minimize the joint error by moving the SMPL joints outside the body (Fig. 2). To avoid such pitfalls, similar to SMPL, we learn a convex combination of vertices  $W'$ , resulting in  $24 \times 6890 = 165,360$  additional learnable parameters and obtain the new joints as  $J' = W'V$ . Visualization in Fig. 3 shows that weights for the learned regressor on Human3.6M shifts from the center of body towards the surface, corresponding to a similar shift in 2D hip landmarks. For the rest of the paper, SJA refers to the learned convex combination of vertices.

### 3.4. Training Losses for the Student

The following losses are used to train the student network via knowledge distillation.

**Knowledge Distillation Loss:** We define a loss between the model-free prediction of 3D joints  $\mathbf{X}_i^j$  and the 3D joints obtained via the SMPL model. To account for the mismatch between the number of joints, we choose  $N$  (14 in our case) relevant joints from the 24 SMPL joints. Let  $\mathcal{I}(i)$  denote the index of the SMPL joint corresponding to  $i^{th}$  input 2D joint.  $\mathcal{L}_{KD}$  is computed as a sum of individual losses over each joint  $i$  and each frame  $j$ ,

$$\mathcal{L}_{KD} = \sum_{j=1}^T \sum_{i=1}^N \|\mathbf{X}_i^j - W'_{\mathcal{I}(i)} \mathcal{M}(\beta, \mathcal{R}^j)\|^2, \quad (7)$$

where  $W'_{\mathcal{I}(i)}$  denote the row of matrix  $W'$  corresponding to the regressor weights for joint  $\mathcal{I}(i)$  and  $\mathcal{R}^j$  denotes the set of predicted rotation matrices for frame  $j$ .

**Regularization of SMPL Parameters:** In absence of any 3D data, we use a simple regularizer for pose parameters to avoid over-twisting by penalizing the deviation of the predicted rotation matrices from identity rotation.

$$\mathcal{L}_\theta = \sum_{j=1}^T \sum_{i=1}^K \|R_i^j - I_{3 \times 3}\|^2, \quad (8)$$

where  $I_{3 \times 3}$  is the  $3 \times 3$  identity matrix. We use a similar  $\mathcal{L}_\beta$  regularizer for  $\beta$ ,  $\mathcal{L}_\beta = \|\beta\|^2$ , since  $\beta = 0$  represents the average human shape. The  $\beta$  regularizer is used

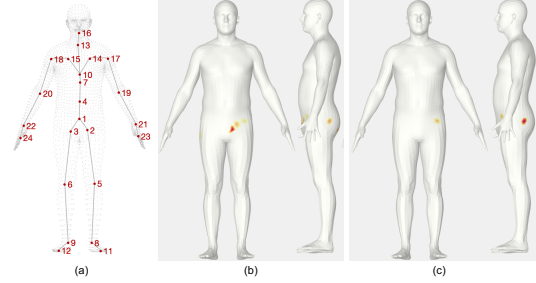


Figure 3: (a) Original SMPL 3D joints (b) SMPL regression weights for the left-hip joint #2 are visualized by assigning a color to each vertex (dark red corresponds to higher weight) (c) Updated regressor weights for hip joint #2 after SJA.

with a relatively larger weight during training to keep the shape close to the average shape. However, we show in Section 4.5 (Fig. 7) that without SJA, these regularizers by themselves are not sufficient to avoid unnatural predictions. Our novel SJA module helps improve the realism and naturalness of predicted pose parameters.

**Discriminator:** Similar to the teacher network, the predicted 3D joints from the student network are reprojected to random views and fed to the discriminator. The corresponding discriminator loss is  $\mathcal{L}_D^S$ , similar to  $\mathcal{L}_D^T$  in Eqn. 5.

### 3.5. Training PoseNet3D

We train PoseNet3D following these steps:

1. Train Teacher: Train the shared temporal convolution backbone and the teacher branch by minimizing  $\mathcal{L}_T = \lambda_{mss} \mathcal{L}_{mss} + \lambda_{tc} \mathcal{L}_{tc} + \lambda_{bl} \mathcal{L}_{bl} + \mathcal{L}_D^T$ .
2. Knowledge Distillation: Freeze the shared temporal backbone and the teacher branch. Train the student branch by minimizing  $\mathcal{L}_S = \mathcal{L}_{KD} + \lambda_R \mathcal{L}_\theta + \lambda_\beta \mathcal{L}_\beta$ .
3. Learn SJA: Initialize  $W'$  to  $W$ . Fine-tune  $W'$  and the student branch by minimizing  $\mathcal{L}_S$ .
4. Fine-tune the entire network by minimizing  $\mathcal{L} = \mathcal{L}_T + \lambda_S \mathcal{L}_S + \mathcal{L}_D^S$ .

Hyper-parameters  $\lambda_{mss}, \lambda_{tc}, \lambda_{bl}, \lambda_R, \lambda_\beta, \lambda_S$  are defined in Sect. 4.1. Note that in step 4, we feed the re-projection of the 3D pose predicted from both the teacher and student networks to the discriminator.

## 4. Experiments and Results

We evaluate on the widely used Human3.6M [22] and MPI-INF-3DHP [40] datasets and show quantitative and qualitative results. We also show qualitative visualizations of reconstructed skeletons and meshes on in-the-wild datasets such as Leeds Sports Pose [26] (LSP) where ground-truth 3D data is not available. Since our approach takes temporal sequences, for inference on single frame input (e.g. LSP), we simply copy the skeleton  $T$  times.

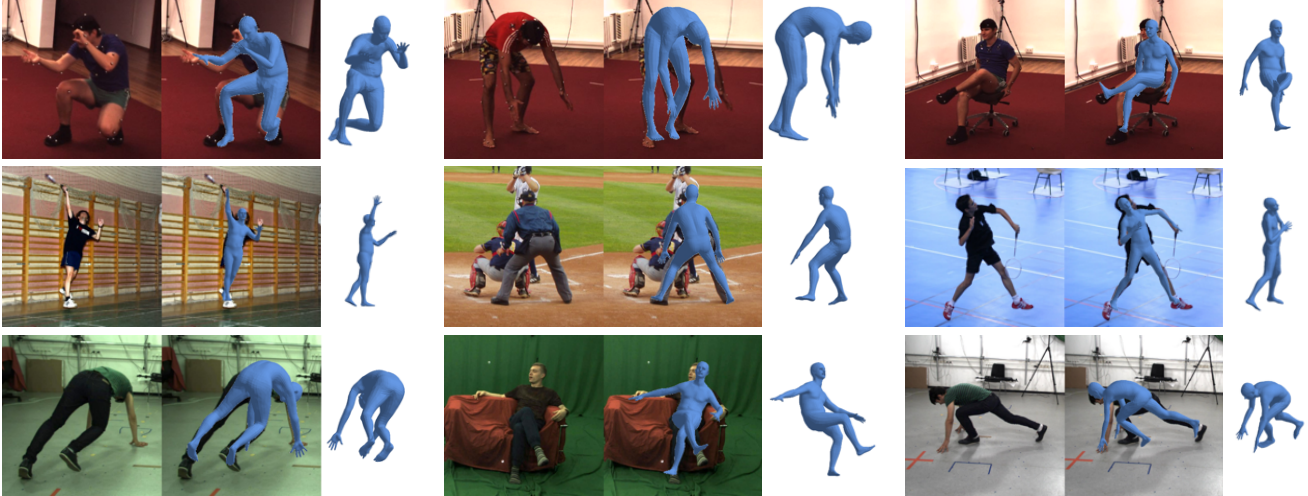


Figure 4: Visualization of SMPL mesh obtained using predicted parameters on challenging examples. Each example shows input image, recovered SMPL mesh, and the same mesh from a different view. The student network is able to recover complicated articulations of the human body. First row: H3.6M. Second row: LSP. Third row: MPI-INF-3DHP.

#### 4.1. Implementation Details

We use  $N = 14$  joints and randomly sample  $T = 9$  frame sub-sequences of 2D poses from video sequences for training. The input poses are normalized such that the mean distance from the head joint to the root joint is 0.1 units, corresponding to placing the 3D skeletons at  $c = 10$  units from the camera. As shown in Fig. 1, our temporal backbone takes a  $2N \times T$  input followed by a *conv-block*, comprising of convolution filter, batchnorm, ReLU and dropout. Each convolution filter has 1024 channels with a kernel size of  $3 \times 1$  and temporal dilation factor of  $d = 1$ . The output of the *conv-block* is fed to a residual block with two *conv-blocks*, with a dilation ratio of  $d = 3$  and  $d = 1$ , respectively. The teacher branch consists of an additional residual block with 2 fully-connected (FC) layers of size 1024 each. Similarly, the student branch consists of 4 FC residual blocks. The temporal discriminator architecture is identical to the temporal backbone architecture but does not use BatchNorm. We train on TitanX GPUs using the Adam optimizer [29] with batchsize of 6000 and learning rate of 0.0001 for 150 epochs. The loss weights are set as  $\lambda_{mss} = 2$ ,  $\lambda_{tc} = 1$ ,  $\lambda_{bl} = 2$ ,  $\lambda_R = 30$ ,  $\lambda_\beta = 10$  and  $\lambda_S = 2$ .

#### 4.2. Datasets and Metrics

**Human3.6M (H3.6M):** This is one of the largest 3D human pose datasets, consisting of 3.6 million 3D human poses. The dataset contains video and MoCap data from 11 subjects performing typical activities such as walking, sitting, etc. Similar to previous works [6, 13, 27], we report the mean per joint position error in mm after scaling and rigid alignment to the ground truth skeleton (P-MPJPE) on subjects S9 and S11 (all cameras). We only use 2D data from

subjects S1, S5, S6, S7 and S8 for training a single activity-agnostic model. To evaluate the smoothness of predicted 3D pose, we report mean per joint velocity error (MPJVE), which is calculated as the mean per joint error of the first derivative of the aligned 3D pose sequences. We also propose the mean bone-length standard deviation (MBLSTD) metric as the average standard deviation (in mm) of 8 bone segments (corresponding to upper/lower/left/right hand/leg) over all sequences. Lower values of MPJPE, MPJVE, and MBLSTD signify better performance.

**MPI-INF-3DHP:** The MPI-INF-3DHP dataset consists of 3D data captured using a markerless multi-camera MoCap system. The ground truth 3D annotations have some noise, which is a known symptom of markerless MoCap systems. We evaluate on valid images from test-set containing 2929 frames following [27] and report P-MPJPE, Percentage of Correct Keypoints (PCK) @150mm, and Area Under the Curve (AUC) computed for a range of PCK thresholds.

#### 4.3. Quantitative Results

We denote our results obtained by taking the average of the predicted 3D poses from the teacher and the student networks as *PoseNet3D*. For a fair comparison with model-free methods in Table 1, we also report the results from the teacher branch (*PoseNet3D-Teacher*) after Step 1 of training (Sect. 3.5). Similarly, results from the student branch after Step 3 of training are denoted as *PoseNet3D-Student* in Table 2. The corresponding results from the two branches after fine tuning (Step 4, Sect. 3.5) are denoted by *PoseNet3D-Teacher-FT* and *PoseNet3D-Student-FT*, respectively.

As evident from Table 1, all variations of our approach trained using H3.6M data outperforms the state-of-the-art unsupervised algorithm of Chen *et al.* [6] (trained using

Supervision	Method	P-MPJPE	
		GT	IMG
Full	Chen and Ramanan [5]	57.5	82.7
	Martinez <i>et al.</i> [39]	37.1	52.1
	IGE-Net [25] (17j)	35.8	47.9
	Li and Lee [34]	-	42.6
	Ci <i>et al.</i> [10]	27.9	42.2
	Hossain & Little [55] (17j) †	-	42.0
	Pavlo <i>et al.</i> [52] †	22.7	40.1
	Cai <i>et al.</i> [3] †	-	39.0
	Yang <i>et al.</i> [69](+)	-	37.7
	Weak/Self	3DInterpreter [66]	88.6
Tung <i>et al.</i> [60]		-	98.4
AIGN [14]		79.0	97.2
RepNet [62]		38.2	65.1
Drover <i>et al.</i> [13]		38.2	64.6
Wang <i>et al.</i> [63]		-	62.8
Kocabas <i>et al.</i> [30](‡)		-	60.2
Unsupervised		Rhodin <i>et al.</i> [56](‡)	-
	Chen <i>et al.</i> [6]	58.0	-
	Chen <i>et al.</i> [6](†)(+)	51.0	68.0
	PoseNet3D-Teacher(†)	50.6	66.6
	PoseNet3D-Teacher-FT(†)	<b>46.7</b>	<u>62.1</u>
	PoseNet3D(†)	47.0	<b>59.4</b>

Table 1: **Human3.6M**. Comparison of P-MPJPE for model-free 3D pose estimation. GT and IMG denote results obtained using ground truth 2D annotations and estimated 2D pose by SH/CPM [44, 65] respectively. Best and second best results are bolded and underlined, respectively. (†) using temporal information, (‡) using multi-view data. (17j) using 17 joints. (+) using additional data for training.

H3.6M only). Our best model reduces the P-MPJPE error from 58mm to 47mm (18% improvement). We also outperform several previous weakly-supervised approaches that use 3D information in training. Similarly, on H3.6M, our results are better than previous model-based approaches such as HMR and SPIN that use unpaired 3D data and produce SMPL meshes as output (Table 2). Finally, Table 3 summarizes results on MPI-INF-3DHP. *PoseNet3D* model trained on H3.6M outperforms HMR [27] and come close to the results from SPIN [31], both of which were trained on MPI-INF-3DHP and used unpaired 3D data for training. This offers a strong evidence that *PoseNet3D* generalizes well to out-of-domain datasets (*e.g.*, in this case trained on H3.6M and tested on MPI-INF-3DHP).

#### 4.4. Qualitative Results

Figure 4 shows overlay of generated mesh using predicted SMPL parameters on the corresponding image, for a few examples from H3.6M, LSP and MPI-INF-3DHP datasets. As discussed earlier, since our approach uses only 2D landmarks and cannot estimate accurate shape, pro-

Method	3D Data (Training)	P-MPJPE
NBF [45]	Paired	59.9
HMR [27] (All/Frontal Cam)	Paired	58.1/56.8
HMR-Video [28]†	Paired	57.8
DenseRaC [67]	Paired	51.4
Kolotouros <i>et al.</i> [32]	Paired	50.1
DenseRaC [67]	Synthetic	48.0
HoloPose [17]	Paired	46.5
Sun <i>et al.</i> [59]	Paired	42.4
SPIN [31]	Paired	41.1
HMR [27](All/Frontal Cam)	Unpaired	67.5/66.5
SPIN [31]	CMU Pose Prior	62.0
PoseNet3D-Student (†)	None	63.7
PoseNet3D-Student-FT (†)	None	<u>60.5</u>
PoseNet3D (†)	None	<b>59.4</b>

Table 2: **Human3.6M**. Comparison of our student network with previous approaches that output SMPL parameters. Best and second best results are bolded and underlined, respectively. Our results use SH [44] for 2D pose inputs. *3D data* refers to the use of additional 3D data during training. (†): using temporal information.

Method	3D Data (for Training)	Training Datasets	Rigid Alignment		
			PCK	AUC	P-MPJPE
Vnecet [41]	Paired	H3.6M+MPI-INF-3DHP	83.9	47.3	98.0
HMR [27]	Paired	H3.6M+MPI-INF-3DHP	86.3	47.8	89.8
DenseRaC [67]	Paired+Unpaired	Synthetic+Various	89.0	49.1	83.5
SPIN [31]	Paired	Various	92.5	55.6	67.5
HMR [27]	Unpaired	H3.6M+MPI-INF-3DHP	77.1	40.7	113.2
SPIN [31]	Unpaired	Various	87.0	48.5	80.4
PoseNet3D	None	H3.6M	81.9	43.2	102.4

Table 3: **MPI-INF-3DHP**. Comparison with previous approaches that output SMPL parameters. Metrics for [27, 31, 41] are taken from [31]. *Various* refers to combination of datasets such as H3.6M, MPI-INF-3DHP and LSP. PCK and AUC: higher is better. P-MPJPE: lower is better.

jected mesh may not align well with the human silhouette in the image. However, note that our approach is able to recover complicated articulations of the human body. Fig. 5 shows predicted 3D skeletons from the teacher network on examples from H3.6M and LSP datasets. Finally, Fig. 6 presents a few failure cases of our approach from H3.6M dataset. Please see supplementary material for additional examples.

#### 4.5. Ablation Studies

Table 4 analyzes the impact of number of frames for the teacher network with and without fine-tuning in terms of MPJVE and MBLSTD metrics. We implemented the approach of Chen *et al.* [6] to compute similar metrics and our 9-frame teacher network outperforms their approach, reducing MPJVE and MBLSTD by more than 60% and 30%, respectively.

For the student branch, we first define two baselines.

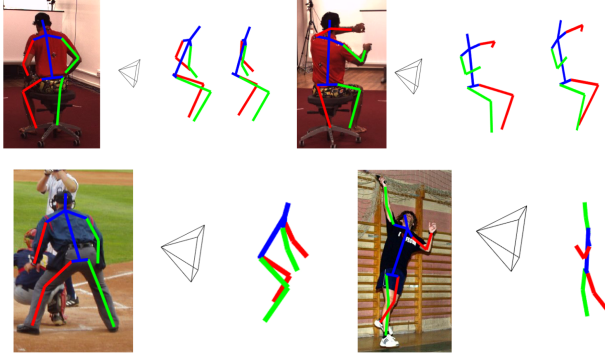


Figure 5: Visualization of predicted 3D pose on H3.6M (top) and LSP (bottom). For H3.6M, the first skeleton in each example shows ground-truth 3D skeleton.

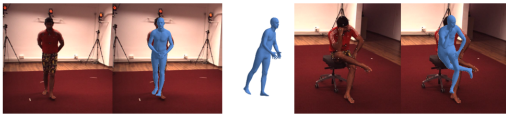


Figure 6: Some failure examples from Human3.6M, depicting front/back depth ambiguity in predicting joints.

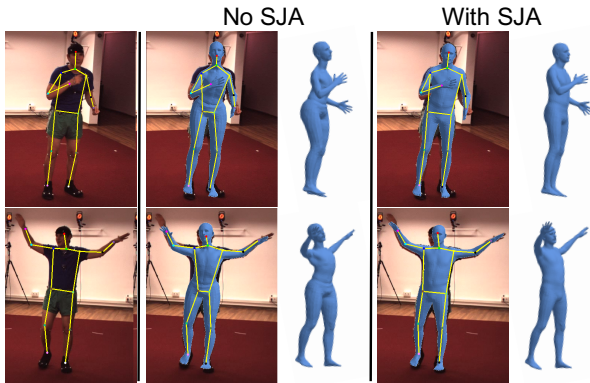


Figure 7: Effect of SJA on the student network.

Ablation	MPJVE	MBLSTD	Student Ablation	P-MPJPE
[6]† (1 frame)	22.2	43.7	Baseline 1	124.8
[6]† (3 frames)	21.0	38.7	Baseline 2	92.5
PoseNet3D-Teacher (1 frame)	23.4	41.6	PoseNet3D-S-LinearSJA	108.4
PoseNet3D-Teacher (9 frames)	13.9	40.1	PoseNet3D-S-NoSJA	70.2
PoseNet3D-Teacher-FT (9 frames)	13.6	38.7	PoseNet3D-S-SJA	63.7
PoseNet3D (9 frames)	<b>7.8</b>	<b>27.0</b>		

Table 4: Ablation studies. (Left) Temporal consistency. (Right) Effect of SJA on student network. Reported metrics use 2D joints obtained from SH [44]. † denotes our implementation of [6].

Since SMPL is a parametric model, a trivial baseline is to train the student network directly by minimizing the 2D re-projection error (*Baseline 1*). We also propose an additional baseline by employing SJA on top (*Baseline 2*). As

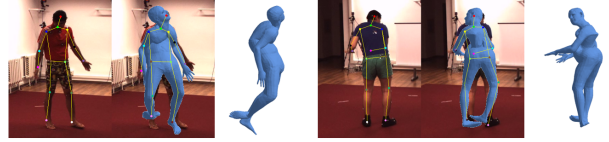


Figure 8: Without knowledge distillation, directly training the student network with 2D re-projection loss results in *monster meshes*, even when the 2D loss is small.

noted in [1] and specifically in [27], minimizing the 2D re-projection error without any 3D supervision can result in *monster meshes* with high P-MPJPE. We observe a similar phenomenon. As shown in Table 4 and Fig. 8, these baselines results in a high P-MPJPE and do not predict high quality poses.

Finally, we analyze the effect of SJA on the student network using KD. Linear-SJA (Eqn. 6) results in low 3D error on training data but high 3D error on test data (*PoseNet3D-S-LinearSJA*). The network severely overfits on the training data by moving joints outside the body (see Fig. 2 for examples). Without using SJA (*PoseNet3D-S-noSJA*), the error is higher than using SJA (*PoseNet3D-S-SJA*). Visualization in Fig. 7 compares the output of student network with and without SJA. Notice how the re-projected 3D skeleton is semantically closer to the input 2D skeleton with SJA (especially hip and head joints). SJA results in better 3D pose predictions confirming that in absence of any paired/unpaired 3D supervision, our semantic joint adaptation module is essential for training the student network.

## 5. Conclusions

We present a knowledge distillation algorithm to learn SMPL pose parameters from 2D joints, without requiring additional 3D data for training. Our approach trains a feed-forward network to predict SMPL parameters and does not require any iterative fitting. We first learn a teacher network to lift 2D joints to model-free 3D pose in a temporally consistent manner. The temporal dynamics are modeled using dilated convolutions in both lifter and discriminator, allowing feedback at every time-step and avoids common pitfalls in using LSTM/RNN in such settings. The teacher network provides pseudo ground-truth to the student network which learns to predict SMPL pose parameters. We demonstrate how to bridge the semantic gap between the SMPL 3D joints and 2D pose landmarks during training, which has been largely ignored in previous literature. We believe that our paper has significantly improved the state-of-art in learning of 3D pose from 2D skeletons in absence of explicit 3D supervision.



## References

- [1] Anurag Arnab, Carl Doersch, and Andrew Zisserman. Exploiting temporal context for 3d human pose estimation in the wild. In *Computer Vision and Pattern Recognition (CVPR)*, pages 3395–3404, 2019. 3, 8
- [2] Federica Bogo, Angjoo Kanazawa, Christoph Lassner, Peter Gehler, Javier Romero, and Michael J Black. Keep it SMPL: Automatic estimation of 3d human pose and shape from a single image. In *European Conference on Computer Vision (ECCV)*, pages 561–578. Springer, 2016. 1, 2, 3
- [3] Yujun Cai, Lihao Ge, Jun Liu, Jianfei Cai, Tat-Jen Cham, Junsong Yuan, and Nadia Magnenat Thalmann. Exploiting spatial-temporal relationships for 3d pose estimation via graph convolutional networks. In *IEEE International Conference on Computer Vision (ICCV)*, 2019. 2, 7
- [4] Zhe Cao, Tomas Simon, Shih-En Wei, and Yaser Sheikh. Real time multi-person 2d pose estimation using part affinity fields. In *Computer Vision and Pattern Recognition (CVPR)*, 2017. 1, 2
- [5] Ching-Hang Chen and Deva Ramanan. 3d human pose estimation = 2d pose estimation + matching. In *Computer Vision and Pattern Recognition (CVPR)*, 2017. 2, 7
- [6] Ching-Hang Chen, Amrith Tyagi, Amit Agrawal, Dylan Drover, Rohith MV, Stefan Stojanov, and James M. Rehg. Unsupervised 3d pose estimation with geometric self-supervision. In *Computer Vision and Pattern Recognition (CVPR)*, 2019. 1, 2, 3, 4, 6, 7, 8
- [7] Xipeng Chen, Kwan-Yee Lin, Wentao Liu, Chen Qian, and Liang Lin. Weakly-supervised discovery of geometry-aware representation for 3d human pose estimation. In *Computer Vision and Pattern Recognition (CVPR)*, 2019. 2
- [8] Yu Cheng, Bo Yang, Bo Wang, Wending Yan, and Robby T. Tan. Occlusion-aware networks for 3d human pose estimation in video. In *IEEE International Conference on Computer Vision (ICCV)*, 2019. 2
- [9] Xiao Chu and Alan Yuille. Orinet: A fully convolutional network for 3d human pose estimation. In *British Machine Vision Conference (BMVC)*, 2018. 1
- [10] Hai Ci, Chunyu Wang, Xiaoxuan Ma, and Yizhou Wang. Optimizing network structure for 3d human pose estimation. In *IEEE International Conference on Computer Vision (ICCV)*, 2019. 7
- [11] Bo Dai, Dahua Lin, Raquel Urtasun, and Sanja Fidler. Towards diverse and natural image descriptions via a conditional GAN. In *IEEE International Conference on Computer Vision (ICCV)*, 2017. 4
- [12] DeepMind. Temporal-3D-Pose-Kinetics. <https://github.com/deepmind/Temporal-3D-Pose-Kinetics>, 2019. 3
- [13] Dylan Drover, Rohith MV, Ching-Hang Chen, Amit Agrawal, Amrith Tyagi, and Cong Phuoc Huynh. Can 3D pose be learned from 2D projections alone? In *ECCV 2018 PeopleCap Workshop*, 2018. 2, 6, 7
- [14] Hsiao-Yu Fish Tung, Adam W. Harley, William Seto, and Katerina Fragkiadaki. Adversarial inverse graphics networks: Learning 2d-to-3d lifting and image-to-image translation from unpaired supervision. In *IEEE International Conference on Computer Vision (ICCV)*, Oct 2017. 2, 7
- [15] David A Forsyth, Okan Arikian, and Leslie Ikemoto. *Computational Studies of Human Motion: Tracking and Motion Synthesis*. Now Publishers Inc, 2006. 1
- [16] I Goodfellow, J Pouget-Abadie, M Mirza, B Xu, D Warde-Farley, and S Ozair. Generative adversarial nets. In *Advances in Neural Information Processing Systems (NIPS)*, pages 2672–2680, 2014. 4
- [17] Riza Alp Guler and Iasonas Kokkinos. Holopose: Holistic 3d human reconstruction in-the-wild. In *Computer Vision and Pattern Recognition (CVPR)*, pages 10884–10894, 2019. 3, 7
- [18] Ikhsanul Habibie, Weipeng Xu, Dushyant Mehta, Gerard Pons-Moll, and Christian Theobalt. In the wild human pose estimation using explicit 2d features and intermediate 3d representations. In *Computer Vision and Pattern Recognition (CVPR)*, 2019. 2
- [19] Kaiming He, Georgia Gkioxari, Piotr Dollár, and Ross Girshick. Mask r-cnn. In *IEEE International Conference on Computer Vision (ICCV)*, pages 2980–2988, 2017. 2
- [20] Geoffrey Hinton, Oriol Vinyals, and Jeff Dean. Distilling the knowledge in a neural network. In *NIPS 2014 Deep Learning Workshop*, 2014. 3
- [21] David Hogg. Model-based vision: a program to see a walking person. *Image and Vision computing*, 1983. 1
- [22] Catalin Ionescu, Dragos Papava, Vlad Olaru, and Cristian Sminchisescu. Human3.6M: Large scale datasets and predictive methods for 3d human sensing in natural environments. *IEEE Transactions on Pattern Analysis and Machine Intelligence*, 36(7):1325–1339, 2013. 5
- [23] Catalin Ionescu, Dragos Papava, Vlad Olaru, and Cristian Sminchisescu. Human3.6M: Large scale datasets and predictive methods for 3d human sensing in natural environments. *IEEE Transactions on Pattern Analysis and Machine Intelligence*, 36(7):1325–1339, Jul 2014. 2
- [24] Karim Isakov, Egor Burkov, Victor S. Lempitsky, and Yury Malkov. Learnable triangulation of human pose. In *IEEE International Conference on Computer Vision (ICCV)*, 2019. 2
- [25] Dominic Jack, Frederic Maire, Sareh Shirazi, and Anders Eriksson. Ige-net: Inverse graphics energy networks for human pose estimation and single-view reconstruction. In *Computer Vision and Pattern Recognition (CVPR)*, 2019. 2, 7
- [26] Sam Johnson and Mark Everingham. Clustered pose and nonlinear appearance models for human pose estimation. In *British Machine Vision Conference (BMVC)*, pages 12.1–12.11, 2010. 5
- [27] Angjoo Kanazawa, Michael J Black, David W Jacobs, and Jitendra Malik. End-to-end recovery of human shape and pose. In *Computer Vision and Pattern Recognition (CVPR)*, pages 7122–7131, 2018. 1, 2, 3, 6, 7, 8
- [28] Angjoo Kanazawa, Jason Y. Zhang, Panna Felsen, and Jitendra Malik. Learning 3d human dynamics from video. In *Computer Vision and Pattern Recognition (CVPR)*, pages 5614–5623, 2019. 7

- [29] Diederik P Kingma and Jimmy Ba. Adam: A method for stochastic optimization. *arXiv preprint arXiv:1412.6980*, 2014. 6
- [30] Muhammed Kocabas, Salih Karagoz, and Emre Akbas. Self-supervised learning of 3d human pose using multi-view geometry. In *Computer Vision and Pattern Recognition (CVPR)*, 2019. 7
- [31] Nikos Kolotouros, Georgios Pavlakos, Michael J. Black, and Kostas Daniilidis. Learning to reconstruct 3d human pose and shape via model-fitting in the loop. In *IEEE International Conference on Computer Vision (ICCV)*, 2019. 2, 3, 7
- [32] Nikos Kolotouros, Georgios Pavlakos, and Kostas Daniilidis. Convolutional mesh regression for single-image human shape reconstruction. In *Computer Vision and Pattern Recognition (CVPR)*, pages 4501–4510, 2019. 7
- [33] Christoph Lassner, Javier Romero, Martin Kiefel, Federica Bogo, Michael J. Black, and Peter V. Gehler. Unite the people: Closing the loop between 3d and 2d human representations. In *Computer Vision and Pattern Recognition (CVPR)*, 2017. 3
- [34] Chen Li and Gim Hee Lee. Generating multiple hypotheses for 3d human pose estimation with mixture density network. In *Computer Vision and Pattern Recognition (CVPR)*, 2019. 2, 7
- [35] Zhi Li, Xuan Wang, Fei Wang, and Peilin Jiang. On boosting single-frame 3d human pose estimation via monocular videos. In *IEEE International Conference on Computer Vision (ICCV)*, 2019. 2
- [36] Junbang Liang and Ming C. Lin. Shape-aware human pose and shape reconstruction using multi-view images. In *IEEE International Conference on Computer Vision (ICCV)*, 2019. 2
- [37] Matthew Loper, Naureen Mahmood, Javier Romero, Gerard Pons-Moll, and Michael J Black. SMPL: A skinned multi-person linear model. *ACM Transactions on Graphics*, 34(6):248, 2015. 1, 4
- [38] Meysam Madadi, Hugo Bertiche, and Sergio Escalera. Smplr: Deep smpl reverse for 3d human pose and shape recovery. *arXiv preprint arXiv:1812.10766*, 2018. 3
- [39] Julieta Martinez, Rayat Hossain, Javier Romero, and James Little. A simple yet effective baseline for 3d human pose estimation. In *IEEE International Conference on Computer Vision (ICCV)*, 2017. 1, 2, 7
- [40] Dushyant Mehta, Helge Rhodin, Dan Casas, Pascal Fua, Oleksandr Sotnychenko, Weipeng Xu, and Christian Theobalt. Monocular 3d human pose estimation in the wild using improved cnn supervision. In *International Conference on 3D Vision (3DV)*, pages 506–516, 2017. 1, 5
- [41] Dushyant Mehta, Srinath Sridhar, Oleksandr Sotnychenko, Helge Rhodin, Mohammad Shafiei, Hans-Peter Seidel, Weipeng Xu, Dan Casas, and Christian Theobalt. Vnect: Real-time 3d human pose estimation with a single rgb camera. *ACM Transactions on Graphics*, 36(4):44, 2017. 2, 3, 7
- [42] Gyeongsik Moon, Ju Yong Chang, and Kyoung Mu Lee. Camera distance-aware top-down approach for 3d multi-person pose estimation from a single rgb image. In *IEEE International Conference on Computer Vision (ICCV)*, 2019. 2
- [43] Francesc Moreno-Noguer. 3d human pose estimation from a single image via distance matrix regression. In *Computer Vision and Pattern Recognition (CVPR)*, July 2017. 2
- [44] Alejandro Newell, Kaiyu Yang, and Jia Deng. Stacked hourglass networks for human pose estimation. In *European Conference on Computer Vision (ECCV)*, pages 483–499, 2016. 2, 7, 8
- [45] Mohamed Omran, Christoph Lassner, Gerard Pons-Moll, Peter Gehler, and Bernt Schiele. Neural body fitting: Unifying deep learning and model based human pose and shape estimation. In *International Conference on 3D Vision (3DV)*, pages 484–494, 2018. 3, 7
- [46] Nicolas Papernot, Martn Abadi, Ifar Erlingsson, Ian Goodfellow, and Kunal Talwar. Semi-supervised knowledge transfer for deep learning from private training data. In *International Conference on Learning Representation*, 2017. 3
- [47] Sunghoon Park, Jihye Hwang, and Nojun Kwak. 3d human pose estimation using convolutional neural networks with 2d pose information. In *European Conference on Computer Vision (ECCV)*, pages 156–169. Springer, 2016. 2
- [48] Sunghoon Park and Nojun Kwak. 3d human pose estimation with relational networks. In *British Machine Vision Conference (BMVC)*, 2018. 2
- [49] Georgios Pavlakos, Nikos Kolotouros, and Kostas Daniilidis. Texturepose: Supervising human mesh estimation with texture consistency. In *IEEE International Conference on Computer Vision (ICCV)*, 2019. 3
- [50] Georgios Pavlakos, Xiaowei Zhou, Konstantinos G. Derpanis, and Kostas Daniilidis. Coarse-to-fine volumetric prediction for single-image 3d human pose. In *Computer Vision and Pattern Recognition (CVPR)*, July 2017. 2
- [51] Georgios Pavlakos, Luyang Zhu, Xiaowei Zhou, and Kostas Daniilidis. Learning to estimate 3D human pose and shape from a single color image. In *Computer Vision and Pattern Recognition (CVPR)*, 2018. 1, 2, 3, 4
- [52] Dario Pavllo, Christoph Feichtenhofer, David Grangier, and Michael Auli. 3d human pose estimation in video with temporal convolutions and semi-supervised training. In *Computer Vision and Pattern Recognition (CVPR)*, pages 7753–7762, 2019. 2, 7
- [53] Haibo Qiu, Chunyu Wang, Jingdong Wang, Naiyan Wang, and Wenjun Zeng. Cross view fusion for 3d human pose estimation. In *IEEE International Conference on Computer Vision (ICCV)*, 2019. 1
- [54] Umer Rafi, Juergen Gall, and Bastian Leibe. A semantic occlusion model for human pose estimation from a single depth image. In *Proceedings of the IEEE Conference on CVPR Workshops*, 2015. 1
- [55] Mir Rayat Imtiaz Hossain and James J Little. Exploiting temporal information for 3d human pose estimation. In *Proceedings of the European Conference on Computer Vision (ECCV)*, pages 68–84, 2018. 7
- [56] Helge Rhodin, Mathieu Salzmann, and Pascal Fua. Unsupervised geometry-aware representation for 3D human pose estimation. In *European Conference on Computer Vision (ECCV)*, 2018. 1, 2, 7

- [57] Gregory Rogez, Philippe Weinzaepfel, and Cordelia Schmid. Lcr-net: Localization-classification-regression for human pose. In *Computer Vision and Pattern Recognition (CVPR)*, July 2017. [2](#)
- [58] Saurabh Sharma, Pavan Teja Varigonda, Prashast Bindal, Abhishek Sharma, and Arjun Jain. Monocular 3d human pose estimation by generation and ordinal ranking. In *IEEE International Conference on Computer Vision (ICCV)*, 2019. [2](#)
- [59] Yu Sun, Yun Ye, Wu Liu, Wenpeng Gao, Yili Fu, and Tao Mei. Human mesh recovery from monocular images via a skeleton-disentangled representation. In *IEEE International Conference on Computer Vision (ICCV)*, 2019. [3](#), [7](#)
- [60] Hsiao-Yu Tung, Hsiao-Wei Tung, Ersin Yumer, and Katerina Fragkiadaki. Self-supervised learning of motion capture. In *Advances in Neural Information Processing Systems (NIPS)*, page 52365246, 2017. [7](#)
- [61] Gul Varol, Duygu Ceylan, Bryan Russell, Jimei Yang, Ersin Yumer, Ivan Laptev, and Cordelia Schmid. Bodynet: Volumetric inference of 3d human body shapes. In *European Conference on Computer Vision (ECCV)*, pages 20–36, 2018. [3](#)
- [62] Bastian Wandt and Bodo Rosenhahn. Repnet: Weakly supervised training of an adversarial reprojection network for 3d human pose estimation. In *Computer Vision and Pattern Recognition (CVPR)*, 2019. [7](#)
- [63] Chaoyang Wang, Chen Kong, and Simon Lucey. Distill knowledge from NRSfM for weakly supervised 3d pose learning. In *IEEE International Conference on Computer Vision (ICCV)*, 2019. [2](#), [3](#), [7](#)
- [64] Jue Wang, Shaoli Huang, Xinchao Wang, and Dacheng Tao. Not all parts are created equal: 3d pose estimation by modelling bi-directional dependencies of body parts. In *IEEE International Conference on Computer Vision (ICCV)*, 2019. [2](#)
- [65] Shih-En Wei, Varun Ramakrishna, Takeo Kanade, and Yaser Sheikh. Convolutional pose machines. In *Computer Vision and Pattern Recognition (CVPR)*, pages 4724–4732, 2016. [2](#), [7](#)
- [66] J. Wu, T. Xue, J. J. Lim, Y. Tian, J. B. Tenenbaum, A. Torralba, and W. T. Freeman. Single image 3d interpreter network. In *European Conference on Computer Vision (ECCV)*, pages 365–382, 2016. [7](#)
- [67] Yuanlu Xu, Song-Chun Zhu, and Tony Tung. DenseRaC: Joint 3d pose and shape estimation by dense render-and-compare. In *IEEE International Conference on Computer Vision (ICCV)*, 2019. [2](#), [7](#)
- [68] I. Zeki Yalniz, Hervé Jégou, Kan Chen, Manohar Paluri, and Dhruv Mahajan. Billion-scale semi-supervised learning for image classification. *CoRR*, abs/1905.00546, 2019. [3](#)
- [69] Wei Yang, Wanli Ouyang, Xiaolong Wang, Jimmy S. J. Ren, Hongsheng Li, and Xiaogang Wang. 3D human pose estimation in the wild by adversarial learning. In *Computer Vision and Pattern Recognition (CVPR)*, July 2018. [7](#)
- [70] Long Zhao, Xi Peng, Yu Tian, Mubbasir Kapadia, and Dimitris N. Metaxas. Semantic graph convolutional networks for 3d human pose regression. In *Computer Vision and Pattern Recognition (CVPR)*, 2019. [2](#)
- [71] Kun Zhou, Xiaoguang Han, Nianjuan Jiang, Kui Jia, and Jiangbo Lu. HEMlets pose: Learning part-centric heatmap triplets for accurate 3d human pose estimation. In *IEEE International Conference on Computer Vision (ICCV)*, 2019. [2](#)